PAPER

Check for updates

A novel P/N/Si/Zn-containing hybrid flame retardant for enhancing flame retardancy and smoke suppression of epoxy resins†

Fangli Li, Ziqin Huang, Changjiang Liu, Meini Yang, Jixiang Wu, Wenhui Rao‡* and Chuanbai Yu [ID] ‡*

Currently, additively efficient flame retardants are being developed to enhance the smoke suppression, flame retardancy, and thermal properties of composite materials. To this end, the current study designed and prepared a novel P/N/Si/Zn-containing organic−inorganic hybrid denoted as APHZ. Its inorganic part was 2-methylimidazole zinc salt (ZIF-8), which improved its smoke suppression and catalytic carbonization. The organic part (P/N/Si-containing compound) promoted its flame retardancy and interfacial compatibility between APHZ and epoxy resin (EP). The test results revealed that EP/APHZ-3 composites achieved a V-0 rating and a notable LOI value of 30.7% when introducing 3 wt% APHZ into the EP matrix. Cone calorimetry tests (CCT) further demonstrated that the average heat release rate (av-HRR), total smoke production (TSP), and CO production (COP) of EP/APHZ-3 were reduced by 23.3%, 14.0%, and 21.1%, respectively. Meanwhile, the char residual was increased by 60.6%, as compared to pure EP. Furthermore, the flame-retardant mechanism of EP/APHZ composites was investigated by the XPS, TG-FTIR, and Raman spectroscopy techniques. The observed synergistic effect of the imidazole skeleton ZIF-8 and P/N/Si-containing compound in APHZ facilitated the generation of a dense multi-element char layer, with the condensed phase flame-retardant mechanism playing a dominant role. These findings contribute to developing and designing high-performance flame-retardant EP.

1. Introduction

Epoxy resins (EPs) are polymers with numerous epoxy groups, typically accompanied by aromatic, aliphatic, and alicyclic chain segments within their main molecular structure.[1] The versatility of EP gives it an extensive spectrum of industrial applications, including coatings, adhesives, electronic equipment, and aircraft due to its excellent electrical insulation, and chemical stability, as well as its diverse set of physical, mechanical, and processing attributes.[2–5] However, EP primarily comprises carbon, hydrogen, and oxygen constituents, rendering it intrinsically prone to flammability, which restricts its potential applications.[6–9]

To solve this problem, flame retardants can be added to the EP matrix to mitigate these combustion-related concerns effectively. Based on chemical composition and mechanism of action, flame retardants can be categorized into organic flame

retardants and inorganic flame retardants. Among them, inorganic flame retardants are known for their excellent thermal stability and smoke suppression, while organic flame retardants and polymers have good compatibility. Combining the advantages of both to obtain low-toxicity and high-efficiency flame retardants is a hot spot for future research.

9,10-Dihydro-9-oxa-10-phosphaphenanthrene-10-oxide (DOPO) and its derivatives are widely used because of their good compatibility with the polymer matrix and good gas-phase fire extinguishing effect.[10–13] For example, Qiu *et al.*[14] researched and developed a new class of phosphaphenanthrene/phenyl siloxane group macromolecules (DDSi-n) for fabricating high-performance epoxy thermosets. Remarkably, when incorporated at an 8% loading level within the EP, the resulting composite (DDSi-n/EP) achieved a vertical combustion test (UL-94) V-0 rating, accompanied by a limiting oxygen index (LOI) value of 34.8%. Furthermore, this incorporation led to a notable enhancement in impact strength by approximately 140%. Jian *et al.*[15] prepared a flame retardant encompassing P/N/S (DOPO-ABZ) by the chemical reaction between DOPO and 2-amino-benzothiazole (ABZ). Upon introducing 7.5 wt% ABZ into EP, DOPO-ABZ achieved a LOI value of 33.5% and successfully achieved a UL-94 V-0 rating. Despite the good flame retardancy of DOPO and its derivatives, several studies have revealed that its smoke suppression properties have not improved.[16–18]

Key Laboratory of New Processing Technology for Non-Ferrous Metals and Materials, Ministry of Education, College of Materials Science and Engineering, Guilin University of Technology (GUT), Guilin 541004, China. E-mail: raowh1@163.com; ycb2008@glut.edu.cn

† Electronic supplementary information (ESI) available. See DOI: https://doi.org/10.1039/d4ra00166d

‡ Both co-authors equally contributed to this study.

2-Methylimidazole zinc salt (ZIF-8), a representative MOF material, has recently been used to modify the resin matrix due to its certain flame retardancy (with high nitrogen content), high specific surface area, and excellent thermal stability.[19–22] The metal oxides generated by the pyrolysis of ZIF-8 can prevent harmful smoke emissions and facilitate the formation of a graphitized char layer structure during burning, thereby safeguarding the underlying polymer.[23,24] Li et al.[25] synthesized a core–shell flame retardant named ZIF-8@BP-Co using ZIF-8 as the core and Co^{2+}-doped borate polymer (BP) as the shell layer. Upon introducing 7.0 wt% ZIF-8@BP-Co into EP, the composites achieved a LOI value of 29.8 ± 0.4% and successfully attained a UL-94 V-0 rating. Furthermore, the peak heat release rate (PHRR), peak total heat release (THR), peak smoke production (PSPR), and total smoke production (TSP) of the composites decreased by 51.3%, 13.2%, 37.2%, and 20.9%, respectively. Liang et al.[26] developed a zeolite imidazolate framework (ZIF-8) with an enhanced nitrogen content, known as N-ZIF-8, by substituting 2-methyl imidazolyl ester with a triazole. This modification aimed to generate more nitrogen-containing compounds to dilute the flammable gas. When 10 wt% N-ZIF-8 was introduced into the rigid polyurethane foam (RPUF), the PHRR of the composite was 465.8 kW m^{-2}, which is 28.8% less than pure RPUF. In addition, the char residual was increased by 17.7%, which shows considerable potential for flame retardant applications. The relatively high additions of flame retardants in these efforts may cause greater damage to other properties of the composite materials. To prepare flame retardants with efficient flame retardancy, good thermal stability, and smoke suppression, an appropriate and feasible strategy is to develop organic/inorganic hybrid flame retardants.

Herein, an organic–inorganic hybrid flame retardant, denoted as APHZ, was designed and prepared by hybridizing ZIF-8 with a P/N/Si-containing compound. ZIF-8 has excellent catalytic carbon formation ability, while the P/N/Si-containing compound is compatible with the EP matrix and has excellent flame retardancy. So APHZ combines both organic flame retardants with excellent compatibility with the polymer matrix and retardancy, as well as the smoke suppression properties and thermal stability of inorganic flame retardants. Subsequently, the effect of APHZ addition on the heat stabilization performances and flame retardancy of EP/APHZ composites was illustrated by diverse test methods, including LOI, UL-94, TGA, and CCT. Additionally, the thermal behavior and flame-retardant mechanisms of EP/APHZ composites were surveyed.

2. Experimental

2.1. Materials

Epoxy resin (E51, epoxy value = of 0.51) was provided by Sinopec (China). 1,5-Diaminonaphthalene and 2-methylimidazole were purchased from Sichuan Xilong Reagent Co., Ltd. (China). Terephthalaldehyde and Zn(NO$_3$)$_2$·6H$_2$O were acquired from Shanghai Aladdin Chemical Reagent Co., Ltd. (China). DOPO was obtained from Guangdong Wengjiang Chemical Reagent
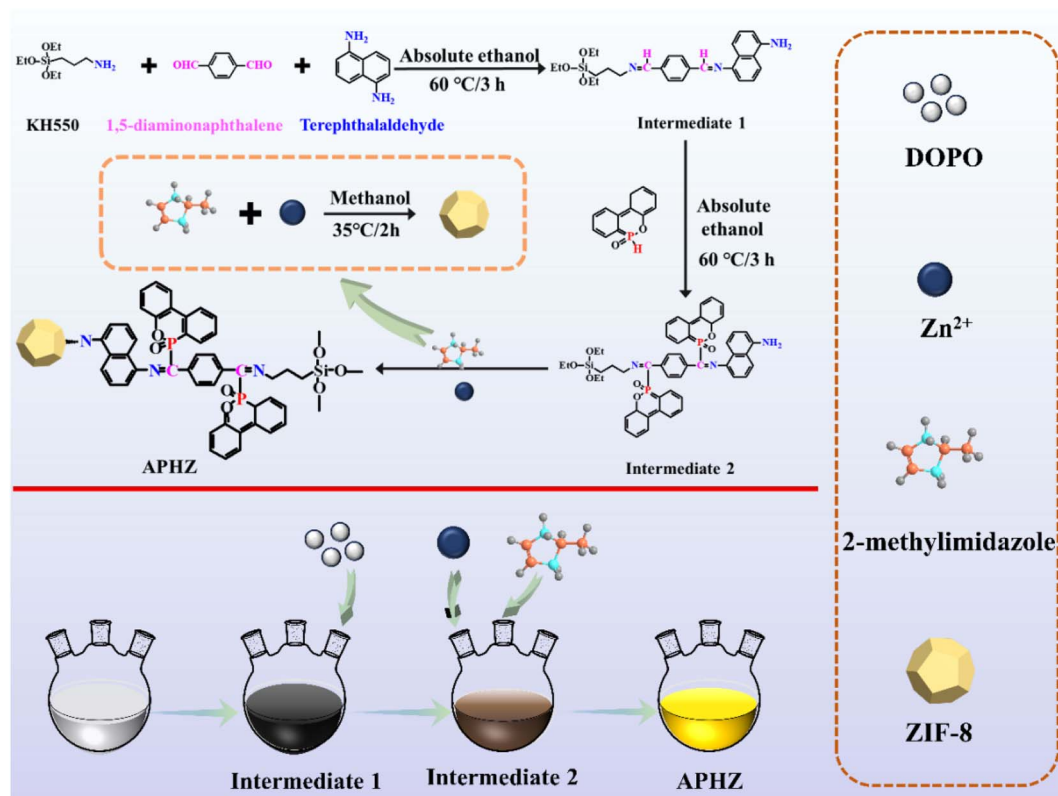
Scheme 1 APHZ fabrication process.

Co., Ltd. (China). 4,4-Diaminodiphenylmethane (DDM) was acquired from Shanghai Macklin Technology Co., Ltd. (China). All chemicals were used without further purification.

2.2. Synthesis of APHZ

First, in a 500 mL flask, 11.07 g of KH550 and 3.95 g of 1,5-diaminonaphthalene were dissolved in 50 mL ethanol, and then sonicated for 10 min. Next, dissolved 10.05 g of 1,4-phthalaldehyde in 100 mL ethanol, added to the above mixture and mixed for 3 h at 60 °C. After that, 1 mol L^{-1} DOPO ethanol solution (100 mL) was added, and the reaction was run at 80 °C for 4 h. In addition, 0.6 mol L^{-1} 2-methylmole methanol solution (100 mL) was added and stirring at 50 °C for 2 h. Finally, a 0.3 mol L^{-1} Zn(NO$_3$)$_2$·6H$_2$O methanol solution was incorporated in the mixture, which was reacted for 2 h at 35 °C, centrifuged, washed several times with methanol, and vacuum

dried at 80 °C for 24 h. The product obtained herein was named as APHZ, the fabrication process of APHZ is shown in Scheme 1.

2.3. Preparation of EP/APHZ composites

The compositions used for the EP/APHZ composites are detailed in Table 1.

The flame retardant (APHZ) was mixed with preheated epoxy resin for an hour at 80 °C using a magnetic stirrer for uniform dispersion. The melted curing agent DDM was incorporated into the system and vacuumed for 10 min. Afterward, Then uniformly prepared mixture was poured into a preheated mold. The curing process was conducted in three stages: first at 80 °C for 2 h, then at 110 °C for 2 h, and finally at 130 °C for 2 h.

2.4. Characterization

Detailed information on characterization is provided in the ESI.†

3. Results and discussion

3.1. Structural characterization of APHZ

Fourier transform infrared (FT-IR) spectra for KH550, DOPO, and APHZ are displayed in Fig. 1(a). For KH550 and DOPO, two characteristic peaks appeared near 3410 cm^{-1} and 1635 cm^{-1}, attributed to the tensile vibration of the –NH and C–H group, respectively.[27] The characteristic peaks at 1203 cm^{-1} and

Table 1 The specific proportions of EP composites

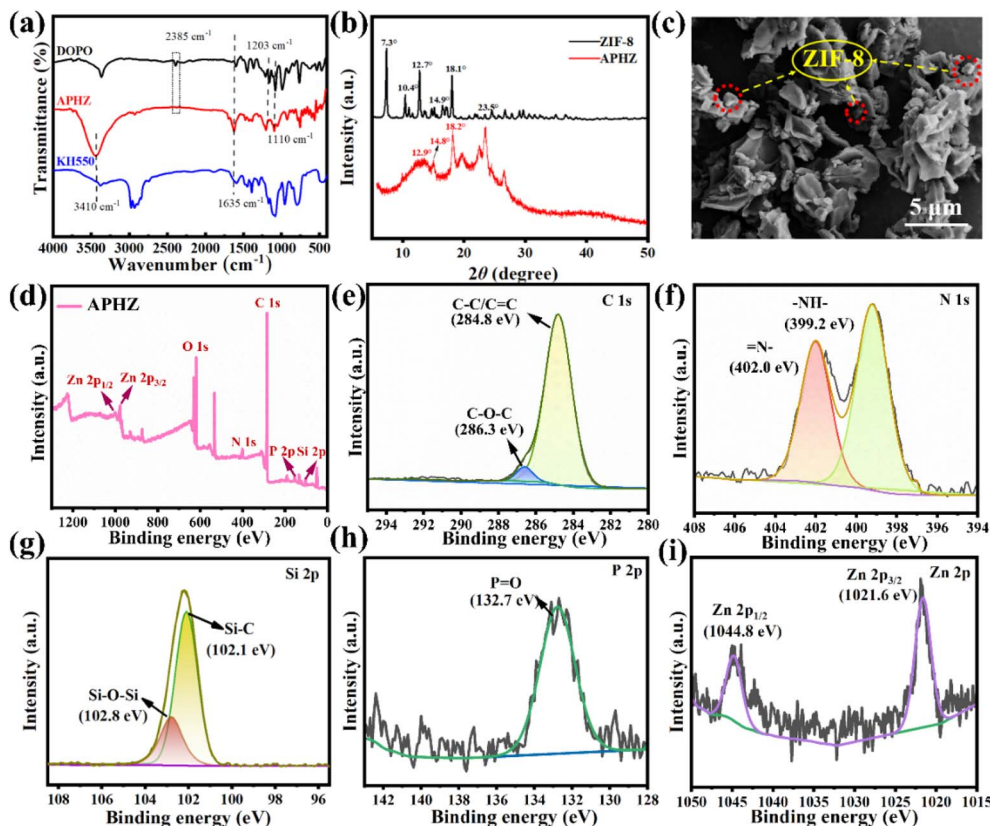| Sample	EP (g)	DDM (g)	APHZ (g)
EP	80.00	20.00	0.00
EP/APHZ-1	80.00	20.00	1.01
EP/APHZ-2	80.00	20.00	2.04
EP/APHZ-3	80.00	20.00	3.09

Fig. 1 FT-IR spectra of KH550, DOPO and APHZ (a), XRD pattern of ZIF-8, APHZ (b), SEM image of APHZ (c), XPS full spectrum (d) and high-resolution C 1s (e), N 1s (f), Si 2p (g), P 2p (h) and Zn 2p (i) for APHZ.

1110 cm^{-1} correspond to the P–O–C group in DOPO and Si–O group in KH50 respectively.[28,29] All these peaks are also discernible in the FT-IR of APHZ. Contrastingly, a notable distinction was observed in the peak at 2385 cm^{-1} (associated with the stretching vibration of P–H in DOPO), which vanished thoroughly in the APHZ spectra. This absence substantiates the occurrence of an aminomethylation reaction during the synthesis process, resulting in the P–H bond disappearance.[30–32]

Fig. 1(b) displays X-ray diffraction (XRD) patterns of ZIF-8 and APHZ. A series of high-intensity diffractions at $2\theta = 17.3°$, 10.4°, 12.7°, 14.9°, and 18.1°, specifically attributed to the (0 1 1), (0 0 2), (1 1 2), (0 2 2), and (2 2 2) planes of ZIF-8, which were consistent with previously reported findings,[33–35] In the XRD analysis of APHZ, characteristic absorption peaks originating from ZIF-8 are observed at $2\theta = 12.9°$, 14.8°, and 18.2°. However, it is noteworthy that the intensity of these diffraction peaks associated with ZIF-8 in the APHZ composite is noticeably reduced. This reduction in peak intensity can be attributed to an amorphous organic compound in the vicinity, which partially masks the crystal structure.[36]

Fig. 1(c) displays the scanning electron microscope (SEM) image of APHZ, which displays several dodecahedral-shaped particles embedded in the amorphous matrix, representing the ZIF-8 hybridized with the intermediate of APHZ.

X-ray photoelectron spectroscopy (XPS) was used to evaluate the chemical valence and elemental composition of APHZ, with the results depicted in Fig. 1(d)–(i). According to XPS's full spectrum of APHZ (Fig. 1d), APHZ mainly comprises C, O, N, Si, P, and Zn elements. The C 1s spectrum in Fig. 1(e) shows the fitting peaks of C–O–C bond and C–C/C=C around 286.3 eV and 284.8 eV,[37] indicating the polyaromatic rings are successfully introduced into APHZ. For the N 1s spectrum (see Fig. 1(f)), two peaks at 399.2 eV and 402.0 eV are associated with –NH– and =N–, respectively. The Si 2p spectrum in Fig. 1(g) was fitted to a pair of peaks corresponding to Si–C (102.1 eV) and Si–O–Si (102.8 eV), respectively. According to the high-resolution P 2p spectrum (Fig. 1h), a pronounced peak at 132.7 eV was observed, being attributed to P=O,[38] which was a strong evidence of the disappearance of the P–H bond due to participation in the reaction. Furthermore, two Zn 2p$_{3/2}$ and Zn 2p$_{1/2}$ fitting peaks are displayed at 1021.6 eV and 1044.8 eV in the Zn 2p spectrum in Fig. 1(i), demonstrating the formation of ZIF-8.[39,40]

The combined FT-IR, XRD, SEM, and XPS results indicated that APHZ was successfully synthesized.

3.2. Thermal properties

The pyrolysis of EP and EP/APHZ composites under a nitrogen atmosphere was analyzed by thermogravimetric analysis (TGA). The correlation curves are plotted in Fig. 2.

Furthermore, the initial degradation temperature ($T_{5\%}$), maximum mass loss rate ($R_{T_{max}}$), maximum degradation temperature (T_{max}), and char residue (C_{700}) of EP and EP/APHZ composites at 30–700 °C are listed in Table 2.

According to Fig. 2(a), the decomposition of both EP and EP/APHZ composites exhibited a one-step decomposition process, with the weight loss mainly occurring from 360 to 460 °C. Introducing APHZ into the EP matrix led to a noticeable effect on the thermal behavior. Specifically, T_{max} for the EP/APHZ composites decreased from 422.7 °C to 413.2 °C. This reduction can be attributed to the decomposition of APHZ and the conversion of phosphates at elevated temperatures. Furthermore, the $R_{T_{max}}$ also experienced a reduction with the incorporation of APHZ. The most significant alteration was observed in the char residue of the EP/APHZ composites when compared to the pure EP. The char residue increased as the mass of APHZ in the composites increased, ranging from 12.3 wt% to 22.0 wt%. This can be elucidated by the generation of polyphosphate, which acted as a promoter in generating a carbonaceous char layer, contributing to the enhanced char residue in the composite.[41–43]

Differential scanning calorimetry (DSC) was employed to assess further the thermal properties of EP and EP/APHZ composites. As depicted in Fig. 2(c), the EP exhibited a glass transition temperature (T_g) of 153.4 °C. However, incorporating 1 wt%, 2 wt%, and 3 wt% of APHZ resulted in noticeable shifts in the T_g values, and the results showed 154.4 °C, 160.4 °C, and 164.5 °C, respectively. This increase in T_g within the EP/APHZ composites is mainly attributed to the presence of six-membered ring structures derived from APHZ. Such structural

Table 2 TGA and DTG data of EP and its composites

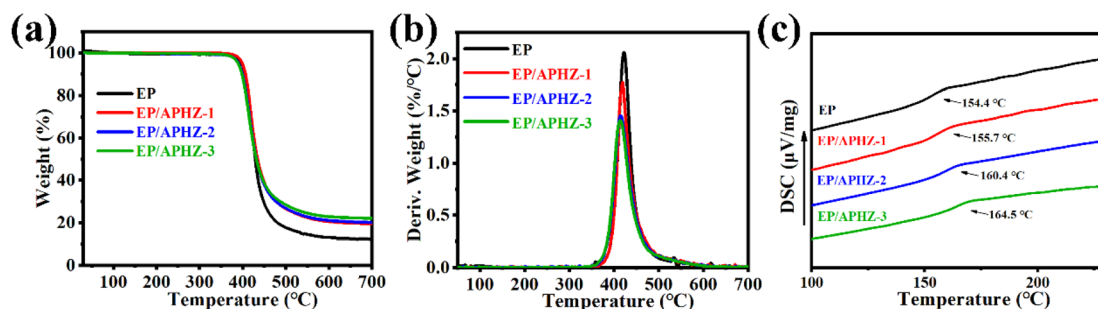| Sample	$T_{5\%}$ (°C)	T_{max} (°C)	$R_{T_{max}}$ (%/°C)	C_{700} (wt%)
EP	397.8	422.7	2.1	12.3
EP/APHZ-1	399.4	419.1	1.8	19.5
EP/APHZ-2	390.4	415.2	1.5	20.2
EP/APHZ-3	389.4	413.2	1.4	22.0

Fig. 2 TGA (a), DTG (b), and DSC (c) curves of EP and its composites.

Table 3 Specific results of UL-94 and LOI testing for EP and its composites

Sample	t_1/t_2 (s)	Rating	Dripping (yes/no)	LOI (%)
EP	206/0	Fail to pass	Yes	23.5
EP/APHZ-1	18/5	V-1	No	28.6
EP/APHZ-2	15/3	V-1	No	29.3
EP/APHZ-3	7/1	V-0	No	30.7

elements contribute to heightened rigidity and elevated heat resistance in EP/APHZ composites, this effect holds significant importance for potential applications requiring enhanced thermal performance.

3.3. Flame retardancy

The utilization of UL-94 and LOI testing methods assessed the flame retardancy of EP composites. The results are listed in Table 3, while digital photographs illustrating the combustion process are given in Fig. 3.

According to Table 3, EP was highly flammable in the air, characterized by a low LOI value of 23.5%, total combustion with molten droplets at 206 s, and failure in the UL-94 test. Comparatively, adding APHZ to the EP matrix significantly improved UL-94 and LOI test results. For instance, adding 1 wt% APHZ resulted in the EP/APHZ composite achieving a V-1 rating, with a combustion time of 23 s and an LOI value of 28.6%. When adding 3 wt% of APHZ, the flame retardancy was improved further, as evidenced by passing the V-0 rating and achieving an LOI value of 30.7%. The results demonstrated that

even a tiny amount of APHZ could significantly improve the flame retardancy of EP/APHZ composites, which can be related to the collaborative influence of multiple elements such as P, N, Si, and Zn within APHZ.

The cone calorimetry test (CCT) was used for evaluating the combustion safety of EP and EP/APHZ composites. Some important data including peak heat release rate (PHRR), average heat release rate (av-HRR), total smoke production (TSP), total heat release rate (THR), heat release rate (HRR), smoke production rate (SPR), CO production rate (COP), and char residues at 700 °C were obtained from CCT. This digital for EP, EP/APHZ-1, and EP/APHZ-3 are displayed in Fig. 4(a)–(f), and the related values are listed in Table 4. According to Table 4, pure EP combines high values of PHRR, av-HRR, THR, TSP, and COP of 1045 kW m^{-2}, 268.7 kW m^{-2}, 83.3 MJ m^{-2}, 34.2 m^2, and 0.038 g s^{-1} respectively explaining its high flammability. These values, however, were generally reduced when APHZ was added, whereas char residual levels increased. For instance, when 3 wt% APHZ was incorporated, the PHRR, THR, and TSP values for EP/APHZ-3 were reduced by 13.1%, 12.1%, and 14.0%, which can be attributed to the P-containing free radicals released by APHZ capture H·, OH· and other highly active free radicals during the combustion process and inhibit the combustion process, proving that the incorporation of APHZ drastically reduces the combustibility of composites.[44] Additionally, the COP represented a 21.1% decrease, while the char residual was increased by 60.6%, which incarnate the catalytic carbon-forming ability of the ZIF-8 in APHZ.[45] Comprehensively, the fire safety of EP is greatly enhanced with the addition of APHZ.
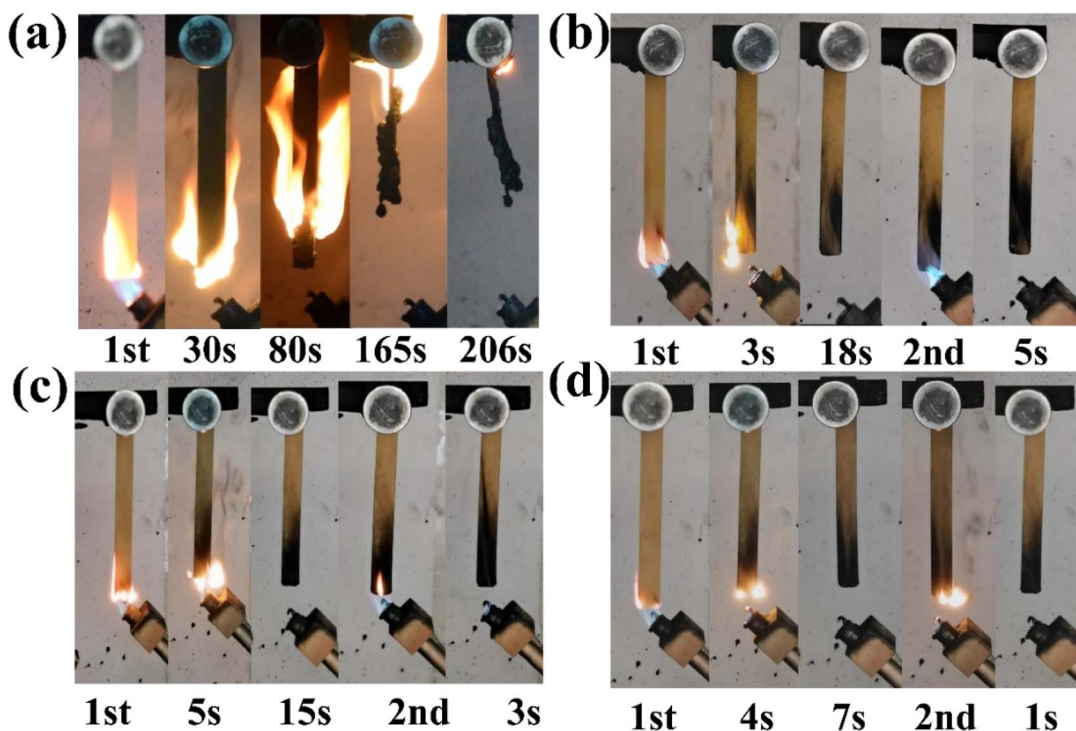

Fig. 3 UL-94 combustion digital images of EP (a), EP/APHZ-1 (b), EP/APHZ-2 (c) and EP/APHZ-3 (d).
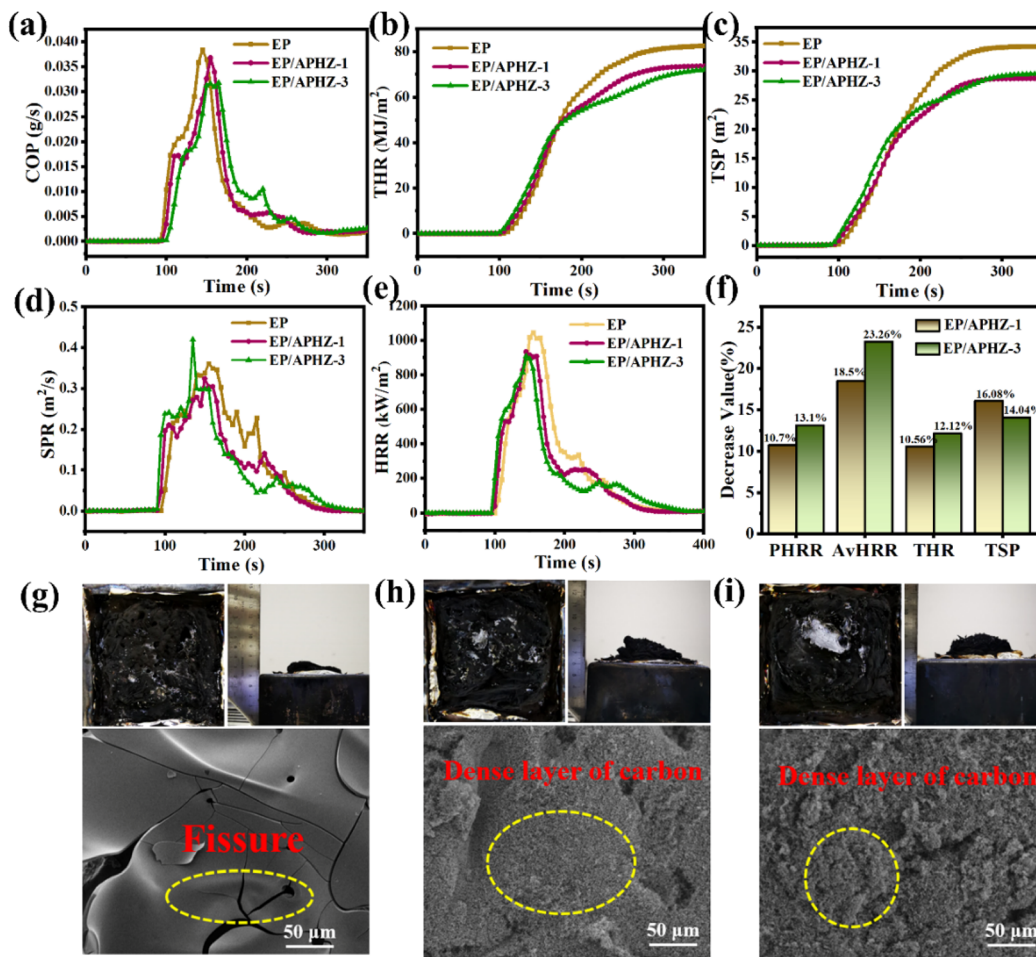
Fig. 4 COP (a), THR (b), TSP (c), SPR (d), HRR (e) curves and downsizings value histogram (f) of EP, EP/APHZ-1 and EP/APHZ-3; digital photos and SEM images of char residue of EP (g), EP/APHZ-1 (h) and EP/APHZ-3 (i) after CCT.

Table 4 Specific results of CCT for EP and its composites

Sample	EP	EP/APHZ-1	EP/APHZ-3
PHRR (kW m^{-2})	1045.0	933.0	907.9
av-HRR (kW m^{-2})	268.7	219.0	206.2
TSP (m^2)	34.2	28.7	29.4
THR (MJ m^{-2})	83.3	74.5	73.2
COP (g s^{-1})	0.038	0.036	0.030
Char residue (wt%)	10.4	16.1	16.7

Digital photos and SEM images of char residue after CCT were observed and comprehensively analyzed for EP, EP/APHZ-1, and EP/APHZ-3, as shown in Fig. 4(g)–(i). From digital photos of char residue after CCT, proved that the volumes of carbon residue for EP/APHZ composites were markedly increased, while the graphitization degree was improved, in comparison with pure EP. As seen in SEM images, the surface of EP appeared to have an evident fissure due to intense combustion, whereas EP/APHZ composites had dense carbon layers instead of fissures. The results could be attributed to the production of polyphosphate during combustion, promoting the formation of

a graphitized carbon layer on the sample surface. This carbon layer acted as a physical barrier, blocking the transfer of heat and flammable gases, thereby reducing the combustion capability of EP/APHZ composites.

3.4. Flame retardancy mechanism

The elemental distribution of char residual after CCT for EP, EP/APHZ-1, and EP/APHZ-3 are shown in Fig. 5.

During the EP combustion, the char residue primarily contained C, N, and oxygen (O) elements. However, in the case of EP/APHZ composites, such additional elements as P, Si, and Zn, were observed in the char residue. Additional elements in the char residue indicate the successful interaction between APHZ and the EP matrix, forming a dense multi-element hybridized char layer during combustion.[46]

The char residue structure of EP and its composites was determined by the Raman spectroscopy. The I_D/I_G ratio reflects the graphitization degree of the char residue, where lower I_D/I_G ratios correspond to a higher graphitization degrees.[47,48] According to Fig. 6(a)–(c), the ID/IG values for pure EP, EP/APHZ-1, and EP/APHZ-3 were 2.9, 2.6, and 2.5, respectively. These results strongly indicate that APHZ incorporation in EP
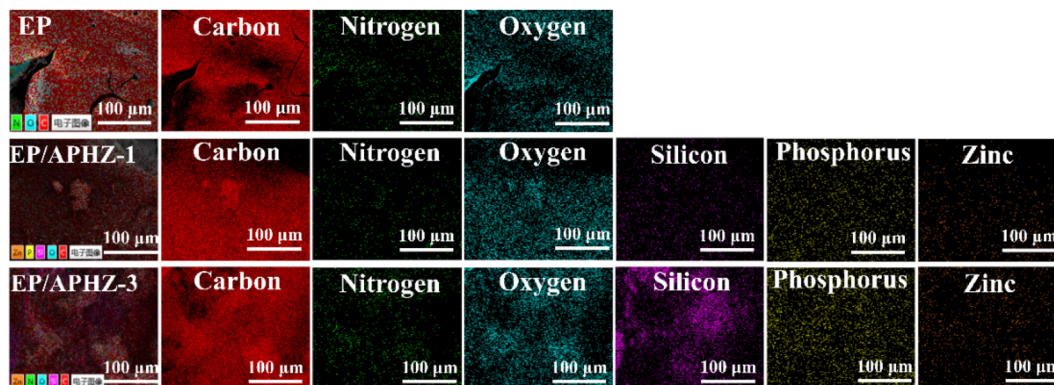
Fig. 5 Element distribution maps of char residue of EP, EP/APHZ-1, EP/APHZ-3 after CCT.

leads to an elevated graphitization degree, improving the flame-retardant performance of composite materials.

The XPS analysis was used to verify the element chemical state of char residuals of EP and its composites. The full spectra of char residuals of EP and EP/APHZ-3 are displayed in Fig. S1,† showing that the char residual of EP/APHZ-3 was primarily composed of C, O, N, Si, and P elements, thus containing two more elements (P and Si), compared to that of EP.

Fig. 6(d)–(f) shows the XPS high-resolution C 1s, Si 2p, and P 2p spectrum of char residue for EP/APHZ-3. According to the high-resolution C 1s spectrum in Fig. 6(d), there were three fitting peaks at 288.9, 286.3, and 284.8 eV, corresponding to C=O, C–O–C, and C–C/C=C,[49] respectively, suggesting a graphitized structure with char residual primally consisting of polycyclic hydrocarbon compounds. The Si 2p spectrum in Fig. 6(e) exhibited two prominent peak values: Si–C (102.8 eV) and Si–O–Si (101.7 eV). As shown in Fig. 6(f), there were PO_3^- and P–O/P=

O peaks around 134.3 eV and 135.6 eV, demonstrating that phosphorus compounds in APHZ burned primarily to form P_2O_5, P_4O_{10}, and polyphosphates.[50] The content of Zn was too low to be detected. Based on these findings, incorporating APHZ in EP would promote a dense multi-element hybridized char layer generation during combustion, preventing further combustion and enhancing the flame-retardant capability of EP composites.

The thermogravimetric-Fourier transform infrared spectroscopy (TG-FTIR) test was used to estimate the gaseous heat degradation products of EP and EP/APHZ composites. Fig. 7(a) and (b) illustrates the 3D diagrams of volatiles released from pure EP and EP/APHZ-3 degradation. Besides Fig. 7(c) and (d) displays their corresponding FTIR spectra at different temperatures.

At approximately 350 °C, the absorption peaks observed in the FTIR spectrum of EP/APHZ-3 correspond to the
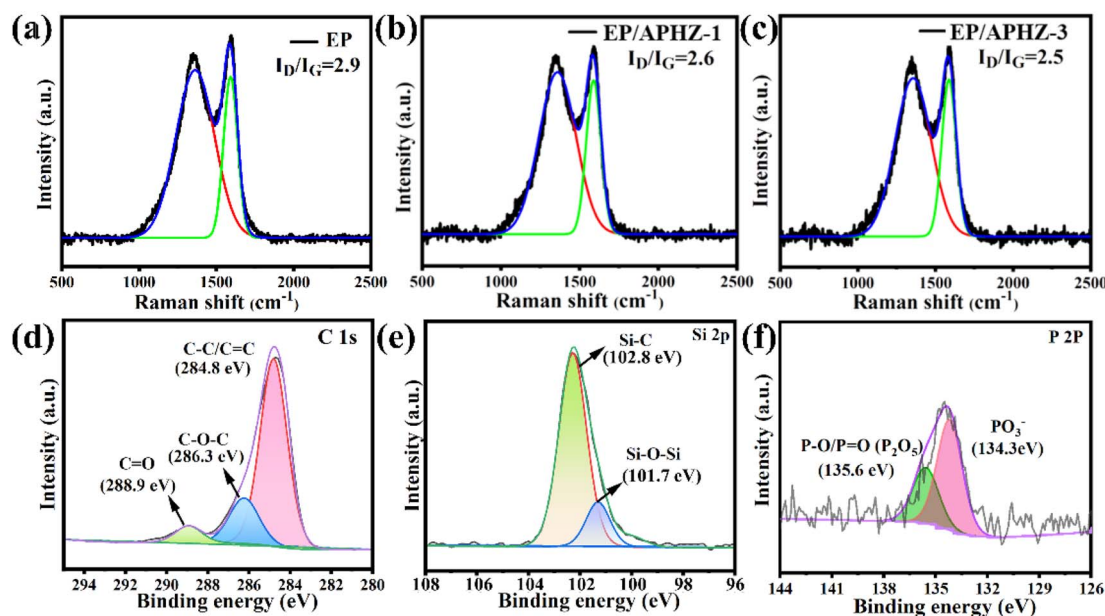

Fig. 6 Raman curves of char residual of EP (a), EP/APHZ-1 (b), and EP/APHZ-3 (c); XPS high-resolution C 1s (d), Si 2p (e) and P 2p (f) spectrum of char residue for EP/APHZ-3.
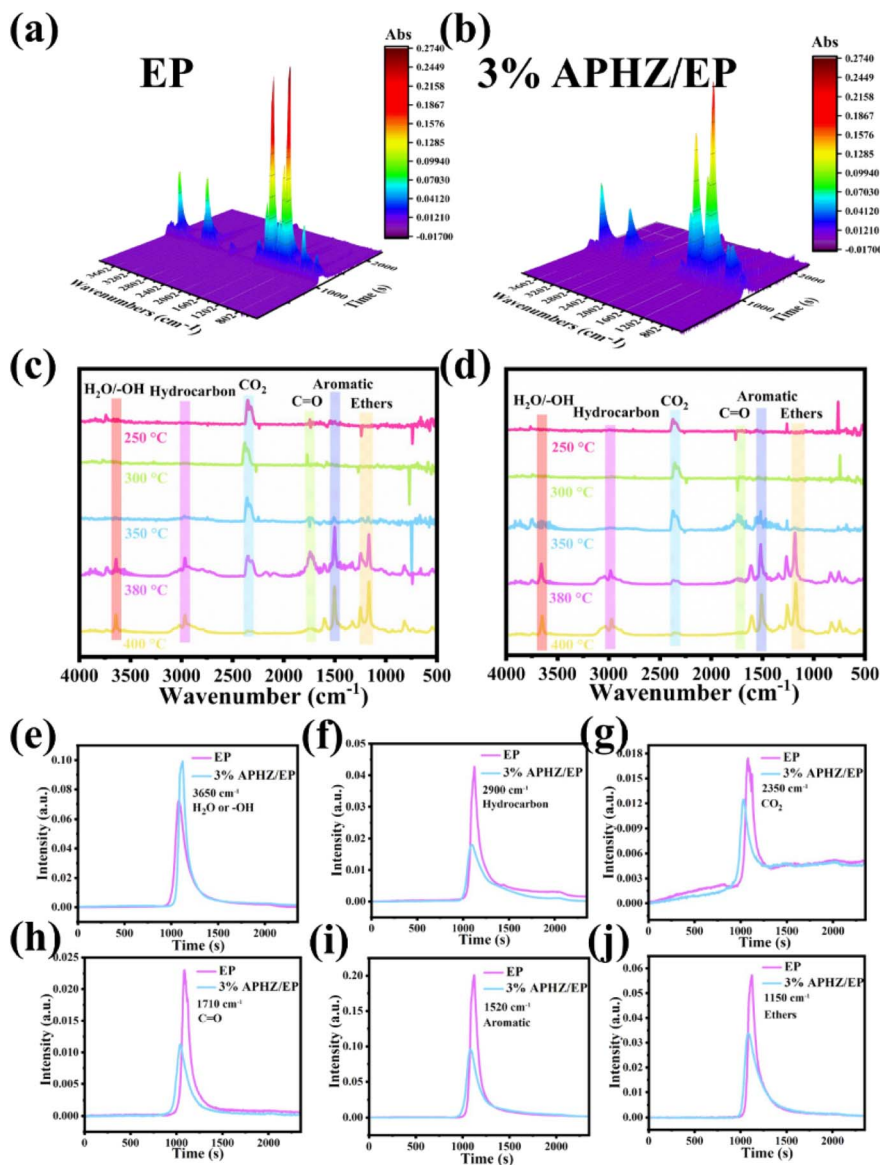
Fig. 7 Three-dimensional total spectra of TG-FTIR test of EP (a) and EP/APHZ-3 (b); FTIR spectra at different temperatures of EP (c) and EP/APHZ-3 (d); intensity of volatiles absorption during pyrolysis of EP and EP/APHZ-3 (e–j) as a function of time.

decomposition of APHZ, as depicted in Fig. 7d. The pyrolysis gas products released from EP/APHZ-3 and pure EP were similar, primarily comprising CO_2 (2350 cm^{-1}), –OH (3650 cm^{-1}), CO (1710 cm^{-1}), aromatic compounds (1520 cm^{-1}), and ethers (1150 cm^{-1}).[51–53] Additionally, it provides an analysis of the gas phase spectra of various compounds, including H_2O (e), hydrocarbons (f), CO_2 (g), carbonyl compounds (h), aromatic compounds (i), and ethers (j). A comparison of the pyrolysis products between EP/APHZ-3 composites and pure EP reveals notable differences in the strengths of typical absorption peaks. Specifically, the intensities of characteristic absorption peaks for CO_2, aromatic compounds, and ethers exhibited a decline in EP/APHZ-3 composites compared to pure EP implying a reduction in the release of potentially flammable and toxic gases. Consequently,

the EP/APHZ-3 composites exhibited enhanced flame retardancy.

The observed flame-retardant mechanism of APHZ in EP composites is illustrated in Scheme 2.

A dense carbon layer can be produced during flaming of EP/APHZ composites, which may be ascribed to the catalytic dehydration of phosphoric acid or polyphosphates obtained by P/N/S-containing compounds, at the catalytic action of ZIF-8. This formation of the dense carbon layer significantly hinders the transfer of heat and flammable substances during combustion. Simultaneously, ZIF-8 can catalyze the conversion of the flammable CO to non-flammable CO_2. Additionally, the ˙PO and ˙HPO_2 produced by P-containing compounds can capture reactive radicals such as ˙H and ˙OH in the gas phase. As a result of the synergistic effect, flame retardancy and smoke suppression were effectively improved. Therefore, based on the
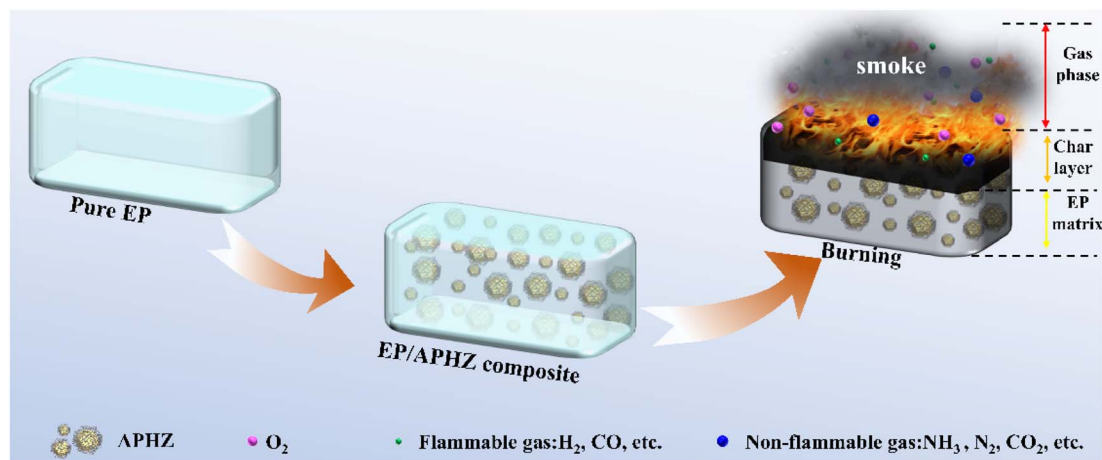
Scheme 2 Flame retardation mechanism of EP/APHZ composites.

above discussion, gas and condensed-phase flame retardant exist simultaneously during combustion, and condensed phase flame retardant plays a dominant role.

4. Conclusions

This study prepared a new organic/inorganic hybrid flame retardant (APHZ) by a multi-element hybridization process and experimentally assessed flame retardancy, smoke suppression behavior, and thermal stability of APHZ/EP composites. The results obtained made it possible to draw the following conclusions:

(1) The proposed APHZ significantly improved the flame retardancy and smoke suppression of EP composites. The composite passed UL-94 V-0 level and achieved a LOI value of 30.7% at 3 wt% APHZ addition, improving thermal stability.

(2) The performed analysis revealed that the condensed phase flame-retardant mechanism dominated during combustion, with APHZ addition causing significant improvement in char residue. Specifically, a dense multi-element hybridized char layer was produced by the synergistic action of ZIF-8 and P/N/Si-containing compound during combustion, effectively hindering heat transfer and flammable gases release, thus improving the flame retardancy and smoke suppression of APHZ/EP composites.

(3) The current study proposed a novel flame retardant method to boost the flame retardancy, smoke suppression, and thermal properties of EP composites, which is considered lucrative for vast potential applications.

Author contributions

Fangli Li: methodology, investigation, writing – original draft. Ziqin Huang: investigation, validation. Changjiang Liu: data curation, material characterization. Meini Yang: conceptualization, investigation. Jixiang Wu: data curation, material characterization. Wenhui Rao: writing – original draft, writing – review & editing. Chuanbai Yu: resources, funding acquisition, supervision, writing – review & editing.

Conflicts of interest

All co-authors declare that they have no conflict of interest.

Acknowledgements

References

1 X. Mi, N. Liang, H. Xu, J. Wu, Y. Jiang, B. Nie and D. Zhang, *Prog. Mater. Sci.*, 2022, **130**, 100977.

2 L. Liu, W. Zhang and R. Yang, *Polym. Adv. Technol.*, 2020, **31**, 2058–2074.

3 Y. Zhang, G. Xu, Y. Liang, J. Yang and J. Hu, *Thermochim. Acta*, 2016, **643**, 33–40.

4 G. Hu, X. Zhang, M. Bu and C. Lei, *Eur. Polym. J.*, 2022, **178**, 111488.

5 H. N. Wang, F. F. Su, Z. H. Wang, Y. Y. Xin, D. D. Yao and Y. P. Zheng, *New J. Chem.*, 2023, **47**, 1760–1766.

6 G. Armstrong and D. Birkett, *Polym. Int.*, 2009, **58**, 969.

7 S. Huo, J. Wang, S. Yang, J. Wang, B. Zhang, B. Zhang, X. Chen and Y. Tang, *Polym. Degrad. Stab.*, 2016, **131**, 106–113.

8 H. Wen and X. Zhang, *IEEE Trans. Dielectr. Electr. Insul.*, 2019, **26**, 1411–1417.

9 G. Venu, J. S. Jayan, A. Saritha and K. Joseph, *Eur. Polym. J.*, 2022, **162**, 110904.

10 H. Luo, F. Zhou, Y. Yang, X. Cao and X. Cai, *J. Therm. Anal. Calorim.*, 2017, **132**, 483–491.

11 Y. Zhang, B. Yu, B. Wang, K. M. Liew, L. Song, C. Wang and Y. Hu, *Ind. Eng. Chem. Res.*, 2017, **56**, 1245–1255.

12 X. Wang, W. He, L. Long, S. Huang, S. Qin and G. Xu, *J. Therm. Anal. Calorim.*, 2020, **145**, 331–343.

13 Y. Wang, W. Kang, X. Zhang, C. Chen, Y. Fu, Y. Fu, Y. Li and F. Zhang, *J. Appl. Polym. Sci.*, 2018, **135**, 45643.

14 Y. Qiu, L. Qian, H. Feng, S. Jin and J. Hao, *Macromolecules*, 2018, **51**, 9992–10002.

15 R. Jian, P. Wang, W. Duan, J. Wang, X. Zheng and J. Wang, *Ind. Eng. Chem. Res.*, 2016, **55**, 11520–11527.

16 S. Yang, Y. Hu and Q. Zhang, *High Perform. Polym.*, 2018, **32**, 137–147.

17 Z. Chi, Z. Guo, Z. Xu, M. Zhang, M. Li, L. Shang and Y. Ao, *Polym. Degrad. Stab.*, 2020, **176**, 109051.

18 D. Shen, Y.-J. Xu, J.-W. Long, X.-H. Shi, L. Chen and Y.-Z. Wang, *J. Anal. Appl. Pyrolysis*, 2017, **128**, 54–63.

19 S. Duan, B. Dou, X. Lin, S. Zhao, W. Emori, J. Pan, H. Hu and H. Xiao, *Colloids Surf., A*, 2021, **624**, 126836.

20 L. Xiong, J. Liu, M. Yu and S. Li, *Corros. Sci.*, 2019, **146**, 70–79.

21 R.-K. Jian, X.-B. Lin, Z. Liu, W. Zhang, J. Zhang, L. Zhang, Z. Li and D. Wang, *Composites, Part B*, 2020, **200**, 108349.

22 M. Taheri and T. Tsuzuki, *ACS Mater. Lett.*, 2021, **3**, 255–260.

23 J. Zhang, Z. Li, L. Zhang, J. García Molleja and D.-Y. Wang, *Carbon*, 2019, **153**, 407–416.

24 J. Zhang, Z. Li, X. Qi, W. Zhang and D.-Y. Wang, *Composites, Part B*, 2020, **188**, 107881.

25 W. Li, Z. Lin, H. Zuo, J. Zhong, Y. Xu, B. Zeng, W. Luo, G. Chen, C. Yuan and L. Dai, *Polym. Degrad. Stab.*, 2022, **198**, 109877.

26 C. Liang, W. Lin, Y. Liu, M. Kang, F. Zhang, W. Qu, S. Li and J. Cheng, *J. Therm. Anal. Calorim.*, 2023, **148**, 9511–9518.

27 A. Mija, C. N. Cascaval, G. Stoica, D. Rosu and B. C. Simionescu, *Eur. Polym. J.*, 1996, **32**, 779–783.

28 B. Yuan, P. Wang, Q. Fang, M. Yang, X. Liu, Z. Tan, Q. Ding, G. Zhang, C. Qi, Z. Gao and J. Mei, *New J. Chem.*, 2023, **47**, 17163–17173.

29 W.-H. Xu, S.-J. Yan and J.-Q. Zhao, *RSC Adv.*, 2022, **12**, 8559–8568.

30 D. Liu, P. Ji, T. Zhang, J. Lv and Y. Cui, *Polym. Degrad. Stab.*, 2021, **190**, 109629.

31 P. Wang and Z. Cai, *Polym. Degrad. Stab.*, 2017, **137**, 138–150.

32 W. Peng, Y.-X. Xu, S.-B. Nie and W. Yang, *RSC Adv.*, 2021, **11**, 30943–30954.

33 X. Y. Lv, W. Zeng, Z. W. Yang, Y. X. Yang, Y. Wang, Z. Q. Lei, J. L. Liu and D. L. Chen, *Polym. Adv. Technol.*, 2020, **31**, 997–1006.

34 W. Xu, G. Wang, Y. Liu, R. Chen and W. Li, *RSC Adv.*, 2018, **8**, 2575–2585.

35 Y. Ma, Y. Sun, J. Yin, H. Sun, H. Wu, H. Wang, Y. Zhang, X. Feng and J. Meng, *J. Taiwan Inst. Chem. Eng.*, 2019, **104**, 273–283.

36 H. Nabipour, S. Nie, X. Wang, L. Song and Y. Hu, *Cellulose*, 2019, **27**, 2237–2251.

37 Z. Li, Z. Liu, J. Zhang, C. Fu, U. Wagenknecht and D. Wang, *Biochem. Eng. J.*, 2019, **378**, 122046.

38 W. Cheng, H. Siqi, Y. Guofeng, W. Bingtao, G. Zhenghong, Z. Qi, S. Pingan, W. Hao and L. Zhitian, *Composites, Part B*, 2023, **268**, 111075.

39 K. Bharti, S. A. Lone, A. Singh, S. Nathani, P. Roy and K. K. Sadhu, *Front. Chem.*, 2021, **9**, 639090.

40 B. Liu, F. Lv, X. Fan, H. Xiao and H. Bi, *Nanomaterials*, 2022, **12**, 748.

41 Z. Huang, B. Ruan, J. Wu, N. Ma, T. Jiang and F. Tsai, *J. Appl. Polym. Sci.*, 2020, **138**, 50413.

42 J. Xu, J. Niu, Z. Xie, F. Liang, F. Guo and J. Wu, *Biochem. Eng. J.*, 2022, **451**, 138566.

43 C. S. Wu, Y. L. Liu, Y. C. Chiu and Y. S. Chiu, *Polym. Degrad. Stab.*, 2002, **78**, 41–48.

44 J. Feng, Y. Lu, H. Xie, Y. Zhang, S. Huo, X. Liu, M. Flynn, Z. Xu, P. Burey, M. Lynch, H. Wang and P. Song, *J. Mater. Sci. Technol.*, 2023, **160**, 86–95.

45 M. Zhang, X. Shi, X. Dai, C. Huo, J. Xie, X. Li and X. Wang, *Asian J. Mater. Sci.*, 2018, **53**, 7083–7093.

46 H. Yu, J. Liu, Z. Wang, Z. Jiang and T. Tang, *J. Phys. Chem. C*, 2009, **113**, 13092–13097.

47 M. Wan, C. Shi, X. Qian, Y. Qin, J. Jing and H. Che, *Nanomaterials*, 2022, **12**, 1142.

48 H. Wang, N. Liu, L. J. Qu and B. S. Xu, *New J. Chem.*, 2023, **47**, 13353–13366.

49 S. Huo, T. Sai, S. Ran, Z. Guo, Z. Fang, P. Song and H. Wang, *Composites, Part B*, 2022, **234**, 109701.

50 Y. Zhang, *RSC Adv.*, 2021, **11**, 34849–34859.

51 C. Yu, T. Wu, F. Yang, H. Wang, W. Rao and H. B. Zhao, *J. Colloid Interface Sci.*, 2022, **628**, 851–863.

52 J. Tao, F. Yang, T. Wu, J. Shi, H.-B. Zhao and W. Rao, *Biochem. Eng. J.*, 2023, **461**, 142061.

53 S. Nie, W. Zhai, Y. Xu, W. He and J. Yang, *RSC Adv.*, 2023, **13**, 29657–29667.